JVST A
Journal of Vacuum Science & Technology A

Impact of precursor concentration on the properties of perovskite solar cells obtained from the dehydrated lead acetate precursors

Cite as: J. Vac. Sci. Technol. A **39**, 032801 (2021); https://doi.org/10.1116/6.0000714
Submitted: 13 October 2020 . Accepted: 09 February 2021 . Published Online: 12 March 2021

Dahiru M. Sanni, Aditya S. Yerramilli, Esidor Ntsoenzok, Sharafadeen A. Adeniji, Omolara V. Oyelade, Richard K. Koech, Adebayo A. Fashina, and Terry L. Alford

COLLECTIONS

Paper published as part of the special topic on Organic, Inorganic, and Hybrid Halide Perovskite Thin Films

View Online Export Citation CrossMark

© 2021 Author(s).

JVST A
Journal of Vacuum Science & Technology A

ARTICLE

avs.scitation.org/journal/jva

Impact of precursor concentration on the properties of perovskite solar cells obtained from the dehydrated lead acetate precursors

Cite as: J. Vac. Sci. Technol. A 39, 032801 (2021); doi: 10.1116/6.0000714
Submitted: 13 October 2020 · Accepted: 9 February 2021 ·
Published Online: 12 March 2021

View Online Export Citation CrossMark

Dahiru M. Sanni,[1,2] Aditya S. Yerramilli,[3] Esidor Ntsoenzok,[4,5] Sharafadeen A. Adeniji,[1,6] Omolara V. Oyelade,[1,7] Richard K. Koech,[5,8] Adebayo A. Fashina,[9] and Terry L. Alford[3,5,a)]

AFFILIATIONS

[1]Department of Theoretical and Applied Physics, African University of Science and Technology, P.M.B. 681 Garki, Abuja 2C2C+9R, Nigeria
[2]Department of Physics, Federal University, P.M.B. 5001 Dutsinma, Katsina State FFCQ+W5, Nigeria
[3]School for Engineering of Matter, Transportation and Energy, Arizona State University, Tempe, Arizona 85282
[4]CEMHTI-CNRS Site Cyclotron, 3A rue de la Férollerie, 45071 Orléans, France
[5]Department of Materials Science and Engineering, African University of Science and Technology, P.M.B. 681 Garki, Abuja 2C2C+9R, Nigeria
[6]Faculty of Natural and Applied Sciences, Nile University of Nigeria, Plot 681, Cadastral Zone C-OO, Research and Institution Area, Jabi, Abuja 900001, Nigeria
[7]Department of Physics, Bingham University, Km. 26, Abuja-Keffi Express Way, P.M.B. 005 Karu, Nasarawa State XM4X+HV, Nigeria
[8]Department of Physics, Moi University, P.O. Box 3900-30100, Eldoret 252, Kenya
[9]Department of Electrical Power Engineering, Gollis University, 26th May District, Hargeisa H28G+3Q, Somaliland

Note: This paper is part of the Special Topic Collection: Organic, Inorganic, and Hybrid Halide Perovskite Thin Films.
[a)]**Author to whom correspondence should be addressed:** TA@asu.edu

ABSTRACT

In this research, we examined the impact of solution concentration on the photovoltaic and the material properties of perovskite solar cells (PSCs) obtained from dehydrated Pb-acetate precursors. The perovskite solution was deposited by a one-step spin-coating technique followed by 5 min of thermal annealing on a hotplate at the temperature of 90 °C to form the perovskite active layer. The PSC device structure adopted was the inverted planar architecture. The precursor solution concentrations were varied from 0.7 to 1.1M, with the optimal solution concentration found to be 1.0M. This concentration results in a power conversion efficiency of 12.2%, an open circuit voltage (Voc) of 0.94 V, a short circuit photocurrent density (Jsc) of 20.71 mA/cm^2, and a fill factor of 62.69%. Our investigations revealed that the precursor solution concentration had a huge effect on the quality of the perovskite film and the photovoltaic properties of the PSCs.

Published under license by AVS. https://doi.org/10.1116/6.0000714

I. INTRODUCTION

Methylammonium lead halide perovskites are unfolding as potential light absorbers for the next-generation solar cell applications. This is due to its numerous advantages, which include long diffusion length, high absorption coefficient, direct bandgap, tunable bandgap, and low cost of production.[1–4] The low cost of production due to its solution processability and the abundance of its constituting materials in nature make it a promising candidate for next-generation solar cell materials.[5] The perovskite solar cells (PSCs) have recorded a high power conversion efficiency (PCE) of about 23%.[6] Different device structures have been used in fabricating PSCs, including mesoporous, regular n-i-p, and inverted p-i-n

Published under license by AVS.

planar architectures. All these device structures have recorded a high PCE.[7–10] The mesoporous structure has some drawbacks in the choice of substrates because of the high processing temperature of over 450 °C,[11] which hinders its applications on flexible substrates.[12] The planar heterojunction architecture, on the other hand, is compatible with a flexible substrate (polymer) because of its low processing temperature below 100 °C.[5,12] Besides the choice of the polymer substrate, the low processing temperature of the planar heterojunction architecture gives it the advantage of choosing a wide range of electrodes and functional layers such as organic holes transport layers [e.g., poly (3,4-ethylene dioxythiophene):poly (styrene sulfonate) (PEDOT:PSS)] and organic electron transport layers [e.g., phenyl-C_{61}-butyric acid methyl ester (PCBM)].[12] Different techniques have been employed in depositing perovskite films such as dip-coating, spray coating, vapor deposition, vapor-assisted solution deposition, one-step spin-coating process, and two-step sequential deposition.[4,5,13–15] Of the various techniques used in the fabrication of perovskites, the one-step spin coating and the two step spin-coating methods are the most widely used methods for the deposition of perovskite films.[16]

Perovskite $CH_3NH_3PbI_3$ films are usually produced by the reaction of CH_3NH_3I and PbI_2 in a ratio 1:1 solution, as shown in Eq. (1). Lead iodide (PbI_2), methylammonium acetate, and methylammonium iodide (MAI) mixed in different ratios were reportedly used as starting precursors for $CH_3NH_3PbI_3$ films.[17] Attempts have also been made in synthesizing $CH_3NH_3PbI_3$ films from nonhalide Pb precursors such as lead acetate [$Pb(OAc)_2$], lead nitrate $Pb(NO_3)$, lead (II) acetylacetonate ($Pb(Ac)_2$, and lead (II) carbonate ($PbCO_3$),[18–26] with $Pb(OAc)_2$ being the most successful of the nonhalide Pb precursor based PSCs.[23,27] The reaction for perovskite formation with lead acetate as a source material is presented in Eq. (2).[28] The reaction in Eq. (2) gives rise to the perovskite film $CH_3NH_3PbI_3$ and the by-product *N*-methylammonium acetate $2CH_3NH_3COO$, which will be evaporated during thermal or solvent annealing,

$$PbI_2 + CH_3NH_3I \rightarrow CH_3NH_3PbI_3, \quad (1)$$

$$Pb(CH_3OO)_2 + 3CH_3NH_3I \rightarrow CH_3NH_3PbI_3 + 2CH_3NH_3COO\uparrow. \quad (2)$$

Despite all the progress made so far on lead-based PSCs, the question of toxicity of the Pb remains key. One way to reduce this risk of toxicity of the lead is by forming an alloy of lead (Pb) and tin (Sn) based perovskite solar cells, i.e., partial substitution of Pb with Sn; this will reduce the lead content in the perovskite film; in case the encapsulation process is compromised, the effect of the lead will be minimal. Sn oxidizes easily in the presence of moisture when heated to form SnO_2, so using nonhalide Pb precursor, like lead acetate trihydrate ($PbAc_2 \cdot 3H_2O$), will be impossible to get a good film of Pb and Sn alloy. For the partial substitution of Pb by Sn to work, the $PbAc_2 \cdot 3H_2O$ has to be processed further to obtain a dehydrated lead acetate [$Pb(Ac)_2$]. The success of the lead-tin (Pb/Sn) based PSCs with lead acetate as the source material will depend largely on the success of the PSCs derived from $Pb(Ac)_2$. Hence, it is important to optimize the processing parameters of the dehydrated lead acetate-based PSCs. Some works have been done with a partial substitution of Pb by Sn,[29,30] which used PbI_2 as the source materials for the $CH_3NH_3PbI_3$ film.

Only a few works have been reported using dehydrated lead acetate [$Pb(Ac)]_2$ as the source material for the fabrication of PSCs. Qing *et al.* employed dehydrated lead acetate to fabricate PSCs; they were able to improve the PCE from 10% to about 12% by using the solvent annealing technique.[25] Sanni *et al.* also used dehydrated lead acetate as the source material to produce PSCs and were also able to improve the PCE from about 10% to 13% by using the preannealing aging approach.[21]

These two works did not report the optimum precursor solution concentration. Based on these works, we used the one-step spin-coating technique to examine the impact of precursor solution concentration on the photovoltaic and material properties of PSCs with $Pb(Ac)_2$ as a Pb source. A p-i-n inverted architecture was used in this research with PEDOT and PCBM as the charge transport layers. Figures 1(a)–1(c) show the J-V curves of devices prepared from different precursor concentrations, the champion device curves, and box plots.

II. EXPERIMENT

A. Materials

The experimental procedure is similar to our previous work.[21] Lead acetate trihydrate ($PbAc_2 \cdot 3H_2O$) was supplied by Alfa Aesar, and MAI was purchased from Dyesol. $Pb(Ac)_2$ was obtained by heating $PbAc_2 \cdot 3H_2O$ in an oven at 78 °C for 1 day. 3.0 mmol of MAI and 1.0 mmol of $Pb(Ac)_2$ were dissolved in 1 ml of dimethylformamide (DMF) to obtain the perovskite solution. Five different solutions were prepared at different MAI and $Pb(Ac)_2$ molar concentrations of 0.7, 0.8, 0.9, 1.0, and 1.1M, respectively. PEDOT:PSS was bought from Ossila, and PCBM was purchased from Sigma Aldrich.

B. Device fabrication

The glass/ITO substrates (Ossila) were sequentially washed in an ultrasonic bath (for 17 min) with a soap solution, de-ionized water, acetone (Sigma Aldrich), and IPA (Sigma Aldrich). The cleaned ITO-glass coated substrates were then blow-dried with flowing nitrogen gas before treating with a UV-ozone for 15 min to remove any organic contaminant left on the substrates. These substrates have dimensions of 2.5 cm by 2.5 cm, with active areas of 0.2 cm^2.

Subsequently, a hole transport layer of PEDOT:PSS was filtered through a 0.45 μm filter (Sigma Aldrich) before spin-coated onto the cleaned ITO-coated glass at the rate of 4000 rpm for 60 s. This was followed by a 16 min thermal annealing on a hotplate at a temperature of 142 °C. These were then transferred into the nitrogen-filled glove box for the perovskite active layer to be deposited. The mixtures of MAI:$Pb(Ac)_2$ dissolved in a DMF were subsequently spin-coated onto the PEDOT:PSS layer at the rate of 4000 rpm for 1 min. This was followed immediately by 5 min thermal annealing at the temperature of 90 °C.

For preparing the electron transport layer (ETL) solution, 20 mg of PCBM powder was dissolved in 1 ml of chlorobenzene. The PCBM:chlorobenzene solution was spin-coated onto the perovskite active layer at the rate of 1000 rpm for 30 s to form the ETL. This layer does not require thermal annealing. The device fabrication

Published under license by AVS.

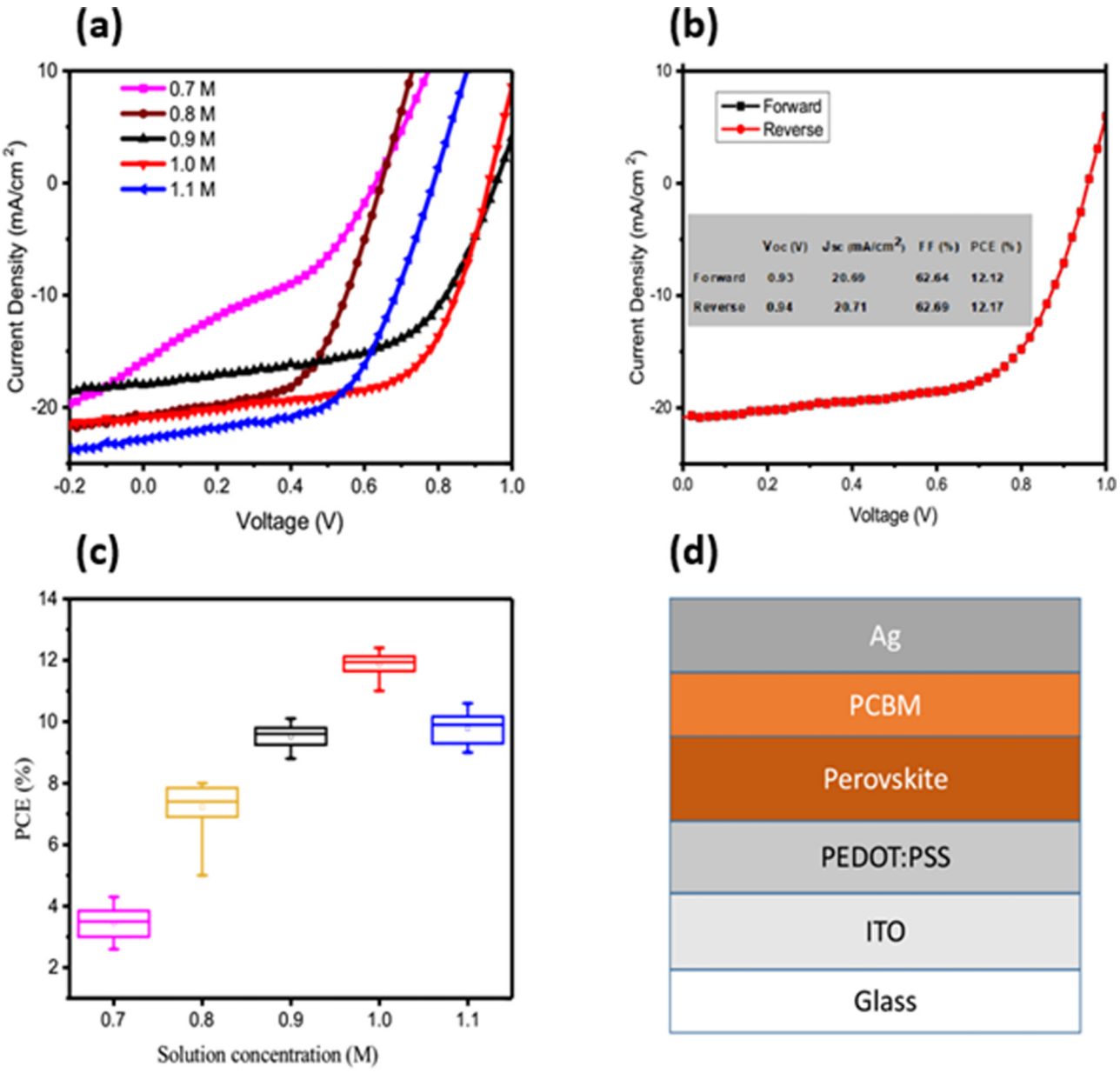

FIG. 1. (a) J-V curves of devices derived from different precursor's concentrations; (b) forward and reverse J-V curves of the champion cell with a solution concentration of 1.0M; (c) box plot of 20 devices with different solution concentrations; and (d) schematic diagram of the inverted PSC structure.

process was completed by thermal evaporation of the silver (Ag) electrode on the ETL. The completed solar cell device has the structure shown in Fig. 1(d).

C. Device characterization

The morphological properties of the as-prepared perovskite samples were observed by XL30 Environmental FEG (FEI) microprobe. The crystalline structure of the perovskite film was analyzed by x-ray diffraction (XRD) measurement at an anode tension of 40 kV and 45 mA filament current to produce the Cu Kα radiation. Scherrer's equation [Eq. (3)] was used to calculate the crystallite size from the dominant peak of the XRD,

$$D = \frac{K\lambda}{\beta \cos \theta}. \quad (3)$$

Published under license by AVS.

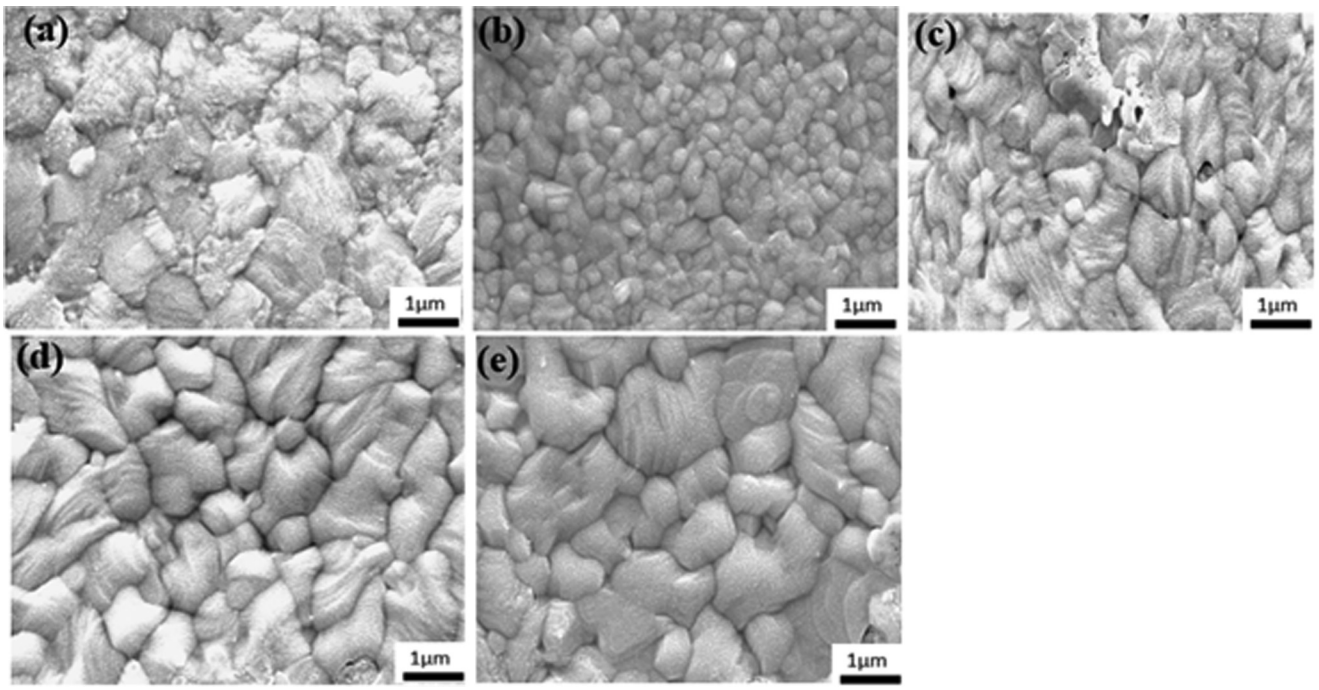

FIG. 2. Surface morphologies of perovskite films derived from different precursor concentrations: (a) 0.7M, (b) 0.8M, (c) 0.9M, (d) 1.0M, and (e) 1.1M.

The optical absorbance was measured by the Cary 5000 UV/VIS spectrometer. The steady-state photoluminescence (PL) spectra of the as-prepared samples were measured with Reinshaw Invia spectroscopy with an ×100 objective lens and 488 nm wavelength as the laser source (Spectra-Physics).

The photovoltaic parameters of PSCs were obtained by carrying out the J-V measurement with an AM 1.5 solar irradiation (100 mW/cm^2) (Spectra-Physics, Oriel Instruments, USA). The film thicknesses were measured with a Dektak 150 surface profilometer.

III. RESULTS AND DISCUSSION

Different solution concentrations were deposited on the PEDOT/ITO/GLASS substrate to obtain various perovskite films. Figure 2 presents the SEM images for the morphologies of the perovskite active layer obtained from different solution concentrations of 0.7, 0.8, 0.9, 1.0, and 1.1M, respectively. The perovskite film derived with a precursor concentration of 0.7M is shown in Fig. 2(a). It is observed that the perovskite film derived from this concentration has poor crystal growth. This is due to the excess DMF solvent in the solution, which requires a much longer time to evaporate the DMF and the by-product methylammonium acetate ($2CH_3NH_3COO$) completely from the perovskite film. This delay in the evaporation time of the DMF and $2CH_3NH_3COO$ leads to a perovskite film with poor crystal growth. In general, since there is more solvent in the low concentration solutions compared to the high concentration solutions, the evaporation rate will be slower compared to samples derived from high concentration solutions; this provides sufficient time for the by-product to decompose in the perovskite film. The delay in the formation of $CH_3NH_3PI_3$ films derived from low solution concentrations has a great effect on the quality of the films produced. It was observed that the crystallinity and the grain sizes of the perovskite films improve with an increase in the solution concentrations up to 1.0M, and beyond this concentration, the crystallinity decreases. The improved crystallinity of the perovskite films with an increase in concentration is due to the rapid evaporation of the solvent and the by-product from the perovskite films, as shown in Fig. 2.

Figure 3(a) shows the XRD patterns of the perovskite active layer obtained from several solution concentrations. From the XRD analysis, the perovskite films produced from solution concentrations of 0.9, 1.0, and 1.1M show obvious diffraction peaks at 14.19 and 28.42, corresponding to peak (110) and (220) lattice planes of the $CH_3NH_3PbI_3$ phase, respectively. The perovskite films prepared with precursor concentrations of 0.9 and 1.0M have additional diffraction peaks at 43.16°, which corresponds to peak (330) lattice planes of the $CH_3NH_3PbI_3$ phase. This peak indicates a better crystallinity compared to films derived from other solution concentrations. The intensity peaks of the XRD patterns shown in Fig. 3(a) rise with an increase in the solution concentrations until an optimum concentration of 1.0M. Beyond this concentration, the XRD intensity decreases. The low-intensity peaks noticed with the solution concentrations of 0.7 and 0.8M are due to excess solvent, which requires a longer time for the films to crystalize, hence providing the opportunity for the by-products to remain in the films.

Published under license by AVS.

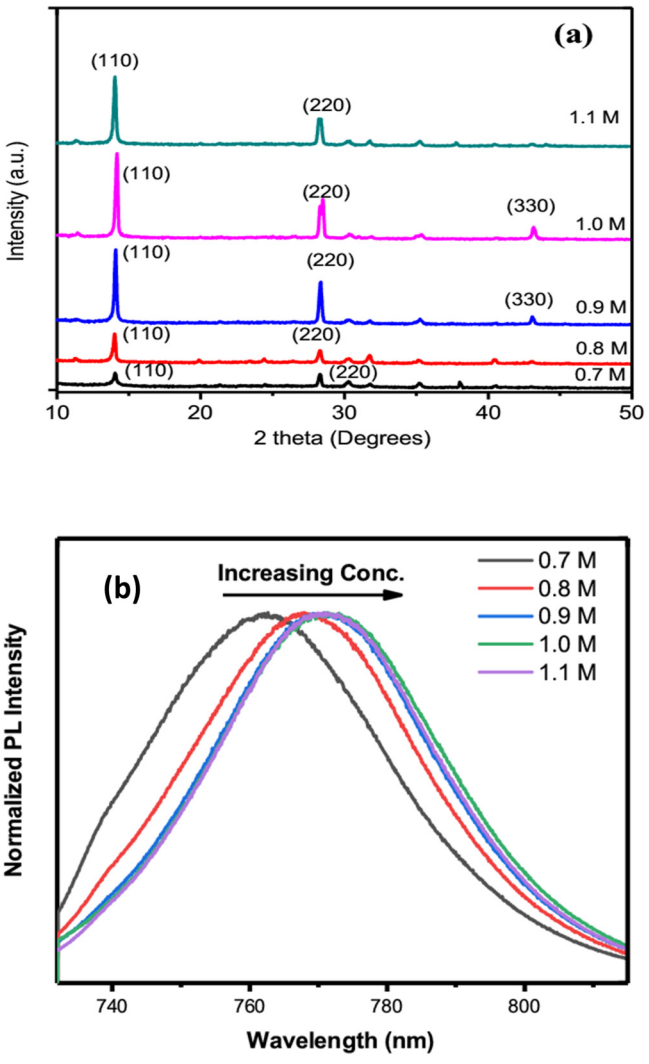

FIG. 3. (a) XRD patterns of the films derived from precursor concentration of 0.7, 0.8, 0.9, 1.0, and 1.1M. (b) Steady-state photoluminescence spectra of perovskite films derived from different solution concentrations.

Scherrer's equation was used for calculating the crystallite sizes from the XRD patterns. The full width at half maximum (FWHM) was calculated from the peak (110) of the XRD patterns. The values of the FWHM and the corresponding crystallite sizes of the various active layers made with different solution concentrations are shown in Table I. The results from Table I show that the crystallite size increases with an increase in solution concentration up to the optimal concentration of 1.0M and also reasonably correlate with the observations from SEM.

The steady-state PL characterization was carried out to investigate further the influence of precursor solution concentration on the performance of $CH_3NH_3PI_3$ films. The PL spectra of the perovskite films spin-coated on glass with different concentrations are shown in Fig. 3(b). The PL intensities were found to be generally similar for all the samples, so they were normalized for better comparison. The films derived from a solution concentration of 0.7 and 0.8M undergo a slight blue shift, which implies an increase in the value of the bandgap of those films. The slight blue shift of the PL spectra of perovskite films could be due to the high content of nonstoichiometric components.[31,32] On the other hand, no red-shift or blue-shift PL spectra are noticed from the films derived from solution concentration of 0.9, 1.0, and 1.1M; this suggests that there is no difference in the bandgap and the grain sizes of the $CH_3NH_3PI_3$ films derived from these concentrations.

TABLE I. FWHM and crystallite size values of the (110) peak for samples derived from different solution concentrations.

Concentration (M)	FWHM	Crystallite size (nm)
0.7	0.076	216.66
0.8	0.065	253.33
0.9	0.062	265.59
1.0	0.057	288.89
1.1	0.059	279.09

Figure 4 shows the UV-vis spectra of the $CH_3NH_3PbI_3$ films prepared on glass substrates with different concentrations. Figure S1 in the supplementary material[44] presents the variation of perovskite film thickness with precursor concentrations. The films were prepared under the same condition except for the precursor concentrations that were varied. The plot shows that the perovskite film thickness increases with an increase in the precursor concentration. This is in agreement with previous similar research.[33–36] The low absorbance noticed in the films prepared with a solution concentration of 0.7M could be due to the low thickness of the photoactive layer. The perovskite film thickness actually increases with an increase in the precursor concentration. The improved light absorption noticed from films prepared with solution concentrations higher than 0.7M could be attributed to the increase in the film thickness as a result of the higher solution concentration and also improved crystallinity of the perovskite films.[37] From Fig. 4(b), it is observed that the perovskite film with a solution concentration of 0.7 M has the best transmittance, and the films derived from solution concentrations of 1.0 and 1.1M have the lowest transmittance. This low transmittance is consistent with the results of Fig. 4(a). The bandgaps were calculated from the absorbance data through Tauc plots (Fig. S2 in the supplementary material[44]). From the calculated values, there is a little increase in the bandgaps for perovskite films prepared with precursor concentrations of 0.7 and 0.8M with corresponding bandgap values of 1.67 and 1.64 eV. The perovskite films prepared with precursor concentrations of 0.9, 1.0, and 1.1M have the same bandgap value of 1.59 eV. These values are consistent with the PL spectra. An increase in the bandgap of perovskite films prepared with precursor concentrations of 0.7 and 0.8M could be due to local chemical inhomogeneity[31,32] as well as a higher content of nonstoichiometric components.[31]

Published under license by AVS.

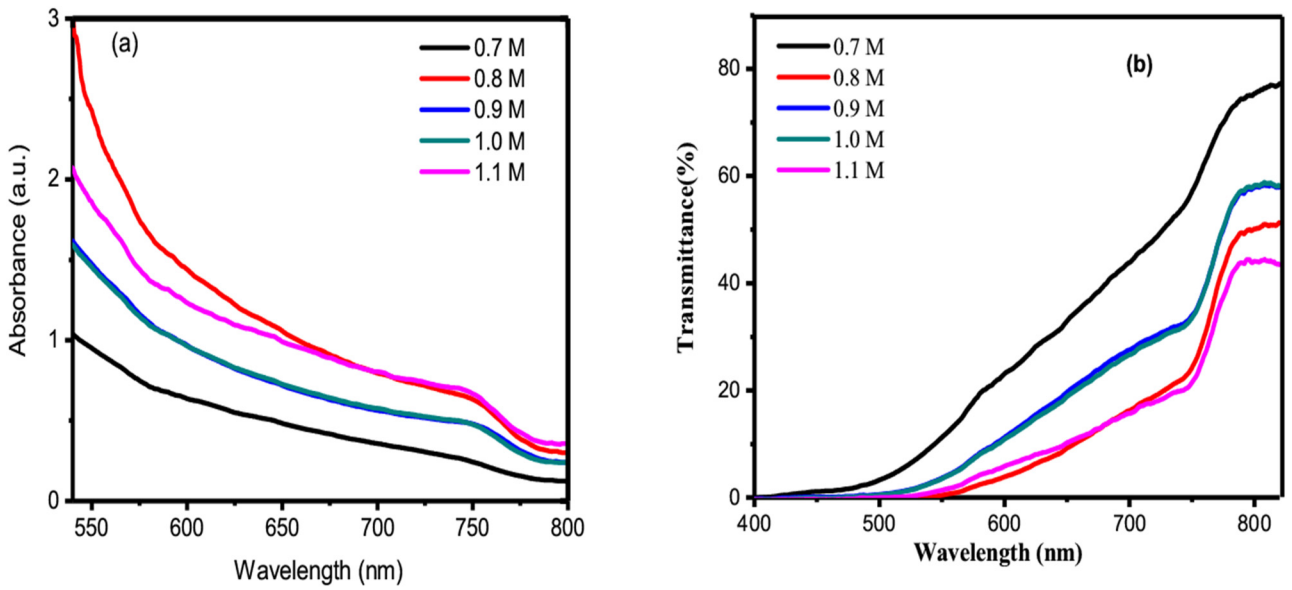

FIG. 4. (a) Absorbance and (b) transmittance spectra of perovskite films derived from precursor concentration of 0.7, 0.8, 0.9, 1.0, and 1.1M.

The device architecture adopted in this research to examine the impact of precursor concentration on the photovoltaic properties is the inverted planar heterojunction architecture p-i-n, as shown in Fig. 1(d). $Pb(Ac)_2$ is used as the Pb source with MAI to obtain the perovskite film ($CH_3NH_3PbI_3$), as stated in Eq. (2). The total PCE of solar cells depends on the Voc, the Jsc, the Fill Factor (FF), and the intensity of the incident light.[38] The J-V curve showing the photovoltaic performance of the PSCs made from different solution concentrations is shown in Fig. 1(a), and Table II shows the device characteristics.

Different precursor concentrations were used in fabricating the device with the structure of glass/ITO/PEDOT:PSS/perovskite/PCBM/Ag. From the J-V curve in Fig. 1(a) and the summary of the photovoltaic properties in Table II, it is observed that the device made from a concentration of 1.0M has the best performing PCE of 12.17%, a Voc of 0.94 V, a Jsc of 20.71 mA/cm^2, and an FF of 62.69%. However, the device made from a solution concentration of 0.7M has the lowest performing PCE of 3.64%, a Voc of 0.63 V, a Jsc of 15.93 mA/cm^2, and an FF of 36.22%. The reason for the low PCE in the device fabricated with a low concentration of 0.7 M could be a result of the excess solvent present in the solution. Hence, it requires a longer time for the by-product to be evaporated out of the perovskite film, giving it enough time to decompose within the film. Also, the low Voc observed in the devices fabricated with a concentration of 0.7 and 0.8M could be due to the by-product ($2CH_3NH_3COO$) present in the film because of its inability to evaporate completely due to the slow evaporation rate. This creates a recombination site between the absorber layer and the transport layers, which imposed a limitation on the value of the Voc. The presence of $2CH_3NH_3COO$ creates defects in the film, which can trap the incident photon, causing parasitic absorption within the active layer that may lead to a low Jsc as a result of the trap-assisted recombination. Also, the low Jsc could be due to the absorber layer thickness, which limits the amount of light it can absorb. This is consistent with the result of the absorbance spectra obtained in Fig. 4(a). More so, the low PCE observed in the device fabricated with a solution concentration of 0.8M could be a result of the small grain sizes, as shown in Fig. 2(b), which means more grain boundaries (GBs) and more defects.[25] The PCE continues to increase with an increase in the precursor solution concentrations up to the optimal concentration of 1.0M. Beyond this point, the PCE decreases. The high PCE observed in the device derived with the concentration of 1.0M could be due to the reduction in trap states in the perovskite film, which gives rise to a good charge carrier mobility because of the smooth, dense uniform film with improved grain size and better crystallinity, which translated into an increase in the values of the Voc, Jsc, FF, and PCE.

The hysteresis experienced during the J-V measurement has shown to be a great problem in perovskite solar cells.[39] In this

TABLE II. Photovoltaic parameters of PSCs derived from different solution concentrations.

Concentration (M)	Voc (V)	Jsc (mA/cm^2)	FF (%)	PCE (%)
0.7	0.63	15.93	36.22	3.64
0.8	0.64	20.82	56.22	7.54
0.9	0.95	18.00	56.44	9.72
1.0	0.94	20.71	62.69	12.17
1.1	0.82	22.91	56.24	10.14

Published under license by AVS.

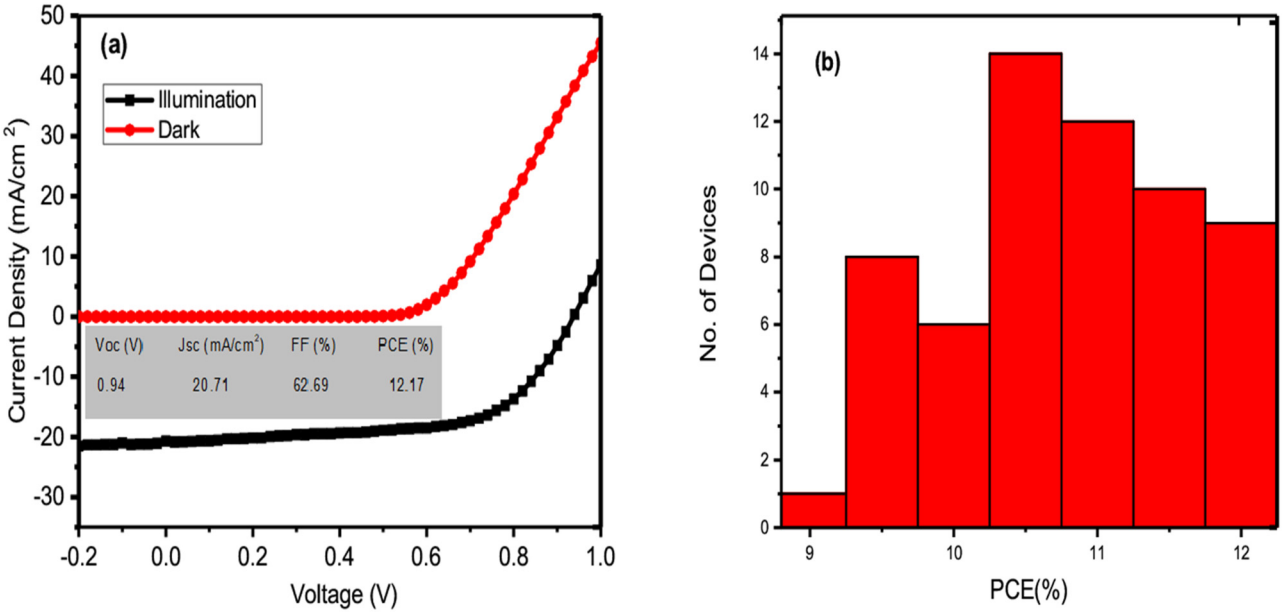

FIG. 5. (a) J-V curve for the champion cell under the illumination of 1.5 AM and in dark conditions. (b) PCE histogram of 60 devices in 12 batches derived from a solution concentration of 1.0M.

research, we studied the hysteresis of the champion cell derived from a solution concentration of 1.0M to be certain of the accuracy of the measurement. We measured the forward and the reverse scan of the J-V curve of the champion cell, as presented in Fig. 1(b), which showed that there is no hysteresis observed. It has been reported that ion migration and trap detrapping process could be responsible for the hysteresis experienced during the J-V measurement of PSCs.[39,40] In the case of the p-i-n structure, the PCBM which are deposited onto the perovskite active layer diffused into the GBs to passivate trap state at the interfaces and suppress the ion migration along the GBs of the perovskite films, which leads to a significant decrease in the hysteresis effect during J-V measurement.[39–43]

The efficiency box plot from 20 devices presented in Fig. 1(c) reveals that the solar cell obtained from a concentration of 1.0M performed better statistically compared to devices derived from other solution concentrations. The superior performance of the devices obtained from the concentration of 1.0M could be due to improved crystallinity of the perovskite active layer.

Figure 5(a) presents the J-V curve of the champion cell under illumination and in the dark, while Fig. 5(b) presents the histogram of the PCE of a device derived from a solution concentration of 1.0M. The repeatability of the champion cell was investigated by preparing 60 devices in 12 batches with a concentration of 1.0M. The average PCE is about $10.5 \pm 0.85\%$, and about 81% of the devices produced have a PCE higher than 10%. The high reproducibility observed from the histogram could be attributed to the quality of the perovskite films, which are smooth and free of noticeable pinholes.

IV. CONCLUSIONS

A one-step spin-coating technique was used to examine the influence of solution concentration on the photovoltaic performance and the materials property of PSCs obtained from $Pb(Ac)_2$ as the Pb source. The study reveals that the concentration of perovskite solution derived from $Pb(Ac)_2$ has a great impact on the photovoltaic and the material properties. The best PCE is obtained to be 12.17% with a solution concentration of 1.0M at an annealing temperature of 90 °C for 5 min. In this research, we were able to investigate the dependency of precursor concentration on the photovoltaic performance of PSCs derived from a $Pb(Ac)_2$ as source material.

ACKNOWLEDGMENTS

This research was supported financially by the Pan African Materials Institute (PAMI) through funding from the World Bank African Centers of Excellence Program (Grant No. AUST/PAMI/2015 5415-NG). The authors are grateful for the support. No conflicts of interests or competing interests exist in the submission of this manuscript.

DATA AVAILABILITY

The data that support the findings of this study are available from the corresponding author upon reasonable request.

REFERENCES

[1]M. A. Green, A. Ho-Baillie, and H. J. Snaith, Nat. Photonics **8**, 506 (2014).

Published under license by AVS.

[2]S. D. Stranks, G. E. Eperon, G. Grancini, C. Menelaou, M. J. P. Alcocer, T. Leijtens, L. M. Herz, A. Petrozza, and H. J. Snaith, Science **342**, 341 (2013).
[3]G. Xing, N. Mathews, S. Sun, S. S. Lim, Y. M. Lam, M. Graïzel, S. Mhaisalkar, and T. C. Sum, Science **342**, 344 (2013).
[4]H. S. Kim *et al.*, Sci. Rep. **2**, 591 (2012).
[5]P. Docampo, J. M. Ball, M. Darwich, G. E. Eperon, and H. J. Snaith, Nat. Commun. **4**, 2761 (2013).
[6]W. S. Yang *et al.*, Science **356**, 1376 (2017).
[7]H. Tan *et al.*, Science **355**, 722 (2017).
[8]M.-H. Liu, Z.-J. Zhou, P.-P. Zhang, Q.-W. Tian, W.-H. Zhou, D.-X. Kou, and S.-X. Wu, Opt. Express **24**, A1349 (2016).
[9]L. Etgar, P. Gao, Z. Xue, Q. Peng, A. K. Chandiran, B. Liu, M. K. Nazeeruddin, and M. Grätzel, J. Am. Chem. Soc. **134**, 17396 (2012).
[10]H. Zhou *et al.*, Science **345**, 542 (2014).
[11]T. C. Sum and N. Mathews, Energy Environ. Sci. **7**, 2518 (2014).
[12]J. You *et al.*, ACS Nano **8**, 1674 (2014).
[13]Q. Chen, H. Zhou, Z. Hong, S. Luo, H. S. Duan, H. H. Wang, Y. Liu, G. Li, and Y. Yang, J. Am. Chem. Soc. **136**, 622 (2014).
[14]J. H. Heo *et al.*, Nat. Photonics **7**, 486 (2013).
[15]J. Burschka, N. Pellet, S. J. Moon, R. Humphry-Baker, P. Gao, M. K. Nazeeruddin, and M. Grätzel, Nature **499**, 316 (2013).
[16]X. Cao, L. Zhi, Y. Jia, Y. Li, K. Zhao, X. Cui, L. Ci, D. Zhuang, and J. Wei, ACS Appl. Mater. Interfaces **11**, 7639 (2019).
[17]S. Venkatesan, M. Hasan, J. Kim, N. R. Rady, S. Sohal, E. Neier, Y. Yao, and A. Zakhidov, J. Mater. Chem. C **5**, 10114 (2017).
[18]A. Buin, P. Pietsch, J. Xu, O. Voznyy, A. H. Ip, R. Comin, and E. H. Sargent, Nano Lett. **14**, 6281 (2014).
[19]D. T. Moore, H. Sai, K. W. Tan, L. A. Estroff, and U. Wiesner, APL Mater. **2**, 081802 (2014).
[20]F. K. Aldibaja, L. Badia, E. Mas-Marzá, R. S. Sánchez, E. M. Barea, and I. Mora-Sero, J. Mater. Chem. A **3**, 9194 (2015).
[21]D. M. Sanni, Y. Chen, A. S. Yerramilli, E. Ntsoenzok, J. Asare, S. A. Adeniji, O. V. Oyelade, A. A. Fashina, and T. L. Alford, Mater. Renew. Sustain. Energy **8**, 3 (2019).
[22]A. S. Yerramilli, Y. Chen, D. Sanni, J. Asare, N. D. Theodore, and T. L. Alford, Org. Electron. **59** 107–112 (2018).
[23]Y. Chen, A. Yerramilli, Y. Shen, Z. Zhao, and T. Alford, Sol. Energy Mater. Sol. Cells **174**, 478 (2018).
[24]T. Y. Hsieh, T. Sen Su, M. Ikegami, T. C. Wei, and T. Miyasaka, Mater. Today Energy **14**, 100125 (2019).
[25]J. Qing, H. T. Chandran, H. T. Xue, Z. Q. Guan, T. L. Liu, S. W. Tsang, M. F. Lo, and C. S. Lee, Org. Electron. **27**, 12 (2015).
[26]M. Sima, E. Vasile, and M. Sima, Mater. Res. Bull. **89**, 89 (2017).
[27]A. S. Yerramilli, Y. Chen, and T. L. Alford, MRS Commun. **1**, 189–193 (2018).
[28]W. Zhang *et al.*, Nat. Commun. **6**, 10030 (2015).
[29]Y. Ogomi *et al.*, J. Phys. Chem. Lett. **5**(6),1004–1011 (2014).
[30]C. C. Stoumpos, C. D. Malliakas, and M. G. Kanatzidis, Inorg. Chem. **52**(15), 9019–9038 (2013).
[31]G. Namkoong, A. A. Mamun, T. T. Ava, K. Zhang, and H. Baumgart, Org. Electron. **42**, 228 (2017).
[32]G. Namkoong, H. J. Jeong, A. Mamun, H. Byun, D. Demuth, and M. S. Jeong, Sol. Energy Mater. Sol. Cells **155**, 134 (2016).
[33]M. Rai, L. H. Wong, and L. Etgar, J. Phys. Chem. Lett. **11**(19), 8189–8194 (2020).
[34]M. I. Alturisa, J. Wira, Herman Mardiyati, and R. Hidayat, J. Phys.: Conf. Ser. **877**, 12046 (2017).
[35]O. K. Ukoba, A. C. Eloka-Eboka, and F. L. Inambao, Energy Procedia **142**, 236 (2017).
[36]J. Raj Mohamed and L. Amalraj, J. Asian Ceram. Soc. **4**, 357 (2016).
[37]Z. Xiao, Q. Dong, C. Bi, Y. Shao, Y. Yuan, and J. Huang, Adv. Mater. **26**, 6503–6509 (2014).
[38]T. Yoshida, S. Fujikake, S. Kato, M. Tanda, K. Tabuchi, A. Takano, Y. Ichikawa, and H. Sakai, Sol. Energy Mater. Sol. Cells **48**, 383 (1997).
[39]Y. Shao, Z. Xiao, C. Bi, Y. Yuan, and J. Huang, Nat. Commun. **5**, 5784 (2014).
[40]J. W. Jung, C. C. Chueh, and A. K. Y. Jen, Adv. Mater. **27**, 7874 (2015).
[41]J. H. Kim, P. W. Liang, S. T. Williams, N. Cho, C. C. Chueh, M. S. Glaz, D. S. Ginger, and A. K. Y. Jen, Adv. Mater. **27**, 695 (2015).
[42]Y. Hou *et al.*, Adv. Mater. **28**, 5112 (2016).
[43]D. M. Sanni, E. Ntsoenzok, E. Saintaimé, S. A. Adeniji, O. V. Oyelade, R. K. Koech, D. I. Amune, and A. Bello, AIP Adv. **10**, 075006 (2020).
[44]See supplementary material at https://doi.org/10.1116/6.0000714 for Figs. S1 and S2.

Published under license by AVS.

View publication stats